Measurement and Correlation of Bubble Point Pressure in (CO_2 + C_6H_6), (CO_2 + $CH_3C_6H_5$), (CO_2 + C_6H_{14}), and (CO_2 + C_7H_{16}) at Temperatures from (293.15 to 313.15) K

E. Nemati Lay*

Department of Chemical Engineering, Faculty of Engineering, University of Kashan, Ravand Street, Kashan, P.O. Box 87317-51167, Iran

The bubble point pressures of (carbon dioxide + benzene), (carbon dioxide + methylbenzene), (carbon dioxide + *n*-hexane), and (carbon dioxide + *n*-heptane) have been measured at CO_2 mole fractions ranging from 0.502 to 0.91 and at temperatures in the range (293.15 to 313.15) K using a pressure−volume−temperature (PVT) apparatus. Also, the effect of temperature and CO_2 concentration on bubble point pressure was investigated. The Peng−Robinson equation of state (PR EOS) with only one binary interaction parameter was used in correlating the experimental data. The results showed that the PR EOS can accurately correlate the experimental data for the bubble point pressure.

Introduction

Recently, supercritical fluid technology has been extensively used to produce fine particles. The most important techniques are, namely, the rapid expansion solution (RESS) process, the particles from gas-saturated solutions (PGSS) process, the supercritical antisolvent (SAS) recrystallization process, the gas antisolvent (GAS) process, precipitation from compressed antisolvent (PCA), solution enhanced dispersion by supercritical fluids (SEDS), and the aerosol solvent extraction system (ASES). These versatile techniques have been applied to generate microparticles as well as nanoparticles which can be more importantly used in pharmaceuticals, polymers, biological-active protein, pigments, catalysts, and superconductor industries.[1−7]

In the GAS process, a compressed gas or a supercritical fluid is introduced into a solution containing the solvent and solute to be micronized. Due to volume expansion in the presence of the antisolvent, the solvent power decreases, and as a consequence, the solute is compelled to precipitate as fine particles.[8] Although many parameters have to be accounted for optimizing these processes, it is clear that the phase behavior of such systems can significantly affect the micronization processes.[9,10] Determination of equilibrium properties of the CO_2−hydrocarbon system not only is essential for production of micro- and nanoparticles but also plays an important role in the energy industries such as CO_2 flooding of petroleum reservoirs and the conversion of coal to liquid fuels.

Vapor−liquid equilibrium data for the (carbon dioxide + benzene), (carbon dioxide + methylbenzene), (carbon dioxide + *n*-hexane), and (carbon dioxide + *n*-heptane) have been published previously, as shown in Table 1.

In this work, the bubble point pressures of (carbon dioxide + benzene), (carbon dioxide + methylbenzene), (carbon dioxide + *n*-hexane), and (carbon dioxide + *n*-heptane) have been measured with a pressure−volume−temperature (PVT) apparatus. Results are reported for these binary systems at CO_2 mole fraction from 0.502 to 0.91, at temperatures in the range (293.15 to 313.15) K. The results obtained were also correlated using the PR EOS with only one binary interaction parameter for each specified system.

Table 1. Published Data for the Binary Systems of (Carbon Dioxide + Benzene), (Carbon Dioxide + Methylbenzene), (Carbon Dioxide + *n*-Hexane), and (Carbon Dioxide + *n*-Heptane) at Different Temperatures, Pressures, and CO_2 Compositions x_1

system	*P*/MPa	*T*/K	x_1	refs
CO_2 + benzene	2.119 to 6.270	313.4 to 393.2	0.017 to 0.661	11
	1.70 to 7.31	293.15 to 308.15	0.230 to 0.979	12
	0.894 to 7.750	298.15 and 313.15	0.1063 to 0.9327	13
	0.105 to 13.295	313.2 to 393.2	0.000 to 0.948	14
	6.895 to 10.960	344.3	0.453 to 0.875	15
	2.29 to 15.39	343.6 and 413.6	0.143 to 0.730	16
	0.826 to 6.313	273.15 to 303.15	0.1238 to 0.9282	17
	7.59 to 10.70	344.3	0.507 to 0.805	18
CO_2 + methylbenzene	0.515 to 6.450	353.4 to 393.2	0.019 to 0.361	11
	1.70 to 7.31	293.15 to 308.15	0.215 to 0.955	12
	0.334 to 15.293	311.25 to 477.05	0.030 to 0.971	19
	0.976 to 5.198	393.25 to 542.85	0.0166 to 0.2261	20
	1.080 to 6.019	323.15 and 333.15	0.080 to 0.889	21
	2.59 to 13.17	353.15 to 413.15	0.012 to 0.783	22
	6.74 to 16.58	333.2 to 572	0.10 to 0.80	23
	0.1 to 5.6	298	0.00 to 0.810	24,25
	0.405 to 12.133	283.15 to 391.45	0.0578 to 0.8871	26
CO_2 + *n*-*n*-hexane	1.70 to 7.31	293.15 to 308.15	0.250 to 0.971	12
	0.444 to 7.657	298.15 and 313.15	0.0495 to 0.9240	13
	1.066 to 6.109	273.15 to 303.15	0.1880 to 0.9019	17
	1.864 to 8.494	303.15 to 323.15	0.1745 to 0.9656	27
	0.779 to 11.597	313.15 to 393.15	0.028 to 0.915	28
	1.824 to 8.461	313.50 and 323.15	0.172 to 0.960	29
	7.184 to 10.369	310.7 to 358.1	0.834 to 0.974	30
CO_2 + *n*-heptane	7.549 to 12.155	313.1 to 370.1	0.885 to 0.958	30
	0.186 to 13.314	310.65 to 477.20	0.022 to 0.949	31
	0.101	283.15 to 313.15	0.01 to 0.014	32
	3.461 to 55.483	301.76 to 459.37	0.2918 to 0.4270	33
	2.30 to 13.40	310.65 to 413.15	0.183 to 0.914	34

Experimental Section

Material. Benzene, methylbenzene, *n*-hexane, and *n*-heptane were supplied by Merck Company. The purity of the chemicals was an estimated mole fraction purity of 0.99 according to the information provided by the supplier. Carbon dioxide with a mole fraction purity of 0.9999 was provided by Air Products Company.

* Corresponding author. E-mail: enemati@kashanu.ac.ir. Tel.: +98 361 5555333. Fax: +98 361 55559930.

10.1021/je900312z CCC: $40.75
Published on Web 08/06/2009

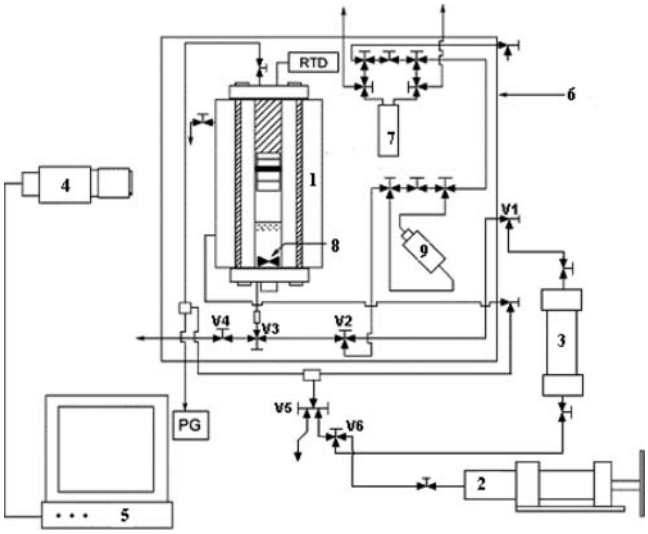

Figure 1. Schematic diagram of the PVT apparatus used in this work: 1, High pressure view cell; 2, High pressure pump; 3, Sample cylinder; 4, CCD camera; 5, Video monitor; 6, Temperature-controlled bath; 7, Densitometer; 8, Mixer; 9, In-line viscometer; RTD, Resistance temperature detector; PG, Pressure gauge.

Apparatus. A schematic diagram of the PVT apparatus (D.B. Robinson Design & Manufacturing Ltd., Edmonton, Canada) was shown in Figure 1. The apparatus is similar to that used by Kho et al.[35] To study the phase behavior and to measure the bubble point pressure of (carbon dioxide + benzene), (carbon dioxide + methylbenzene), (carbon dioxide + *n*-hexane), and (carbon dioxide + *n*-heptane), an apparatus containing the PVT cell was used. The PVT apparatus consists of a high accurate temperature-controlled air bath with an uncertainty of ± 0.1 K that houses a high-pressure variable view cell, with total sample volume of 130 cm^3 rated to an upper pressure of 70 MPa and temperature of 473.15 K, equipped with a magnetic mixer and a low volume sampling port. The pressure of the system was measured with a digital pressure indicator, Heise model 901 A, with an uncertainty of ± 0.05 MPa. The temperature of the air bath unit and the PVT cell is measured with two platinum 100 Ω resistance thermocouples with uncertainty ± 0.3 K. The volume of the fluid phase in the PVT cell can be measured using a charge-coupled device (CCD) camera-based measurement system with uncertainty of ± 0.01 cm^3. Pressurization of the PVT cell can be achieved via a computer-controlled, high-pressure positive displacement pump with a volume resolution of 0.01 cm^3. The apparatus also features a high-pressure densitometer (Anton Paar; model DMA 512P) rated for use at pressures up to 70 MPa and at temperatures of 423.15 K and an in-line electromagnetic viscometer (Cambridge Applied Systems, Medford, MA; model SPL440) rated for operation up to pressures of 140 MPa and temperatures of 463.15 K, at viscosities in the range of (0.1 to 10 000) mPa·s.

The apparatus was also privileged with the real time data acquisition system. The data acquisition system not only supports all the standard instruments in the PVT apparatus including pressure, temperature, volume, density, and viscosity measurements but also provides a full control system for pumping operation.

Procedure. Before beginning the experiments, the lines, sample cylinder, and PVT cell were cleansed, dried, and evacuated. First a known amount of solvent was weighed using a balance with the accuracy of ± 1 mg and charged into the view cell using a high-pressure positive displacement pump with volume resolution of 0.01 cm^3. Then a known amount of CO_2 was charged into the evacuated and balanced standard bomb (S.S.316, 75.0 cm^3 volume, rated up to 12 MPa). Next, a sufficient amount of CO_2 was injected to the view cell from a standard bomb, and the cell was set into a constant-temperature bath. The exact amount of CO_2 charged into the view cell can be calculated from balancing of a standard bomb before and after CO_2 injection. The estimated accuracy of mixture composition data was determined ± 0.001 in mole fraction. In the worst cases, depending on the composition of the mixture, the accuracy of the mixture composition data was ± 0.002 in mole fraction. The solution was mixed vigorously using the magnetic mixer, and the pressure of the system was increased using a high-pressure displacement pump until the mixture was completely liquefied. Then the pressure of system was decreased until a bubble was observed, and the bubble pressure was determined from the pressure at which a small bubble first appeared in the liquid phase. By changing operational conditions such as temperature and CO_2 concentration, the bubble pressure curves can be determined.

Modeling. The PR EOS was used to correlate the bubble point pressure data obtained in this work.[36] The PR EOS can be given by the following equation

$$P = \frac{RT}{v - b} - \frac{a}{v(v + b) + b(v - b)} \tag{1}$$

The parameters of the PR EOS can be obtained using the following quadratic mixing rules

$$a = \sum_i^n \sum_j^n x_i x_j \sqrt{a_i a_j}(1 - k_{ij}) \tag{2}$$

and

$$b = \sum_i^n x_i b_i \tag{3}$$

where x_i is the mole fraction of component i and k_{ij} is the binary interaction parameter for an $i-j$ pair.

The absolute relative deviation percent (ARD %) and average absolute relative deviation percent (AARD %) were minimized to obtain the values of the binary interactions according to the following equations

$$\text{ARD \%} = \left|\frac{P_b^{exp} - P_b^{cal}}{P_b^{exp}}\right| \cdot 100 \tag{4}$$

$$\text{AARD \%} = \left(\frac{\sum_i^N \left|\frac{P_{bi}^{exp} - P_{bi}^{cal}}{P_{bi}^{exp}}\right|}{N}\right) \cdot 100 \tag{5}$$

where P_b and N are the bubble point pressure and the number of experimental points, respectively. The superscripts exp and cal denote the experimental and calculated values, respectively.

Results and Discussion

Tables 2 and 3 report the bubble point pressure of (carbon dioxide + benzene), (carbon dioxide + methylbenzene), (carbon dioxide + *n*-hexane), and (carbon dioxide + *n*-heptane). The data reported in the Table 2 were measured at carbon dioxide mole fractions ranging from 0.502 to 0.91, at temperatures in the range (293.15 to 313.15) K. As seen from Table 2, the bubble point pressure of each binary system used in this work increases as the temperature of the system increases. It is worth mentioning that the experiments were replicated three times,

Table 2. Experimental Bubble Point Pressure P_b and Estimated Uncertainty U_i for (Carbon Dioxide + Benzene), (Carbon Dioxide + Methylbenzene), (Carbon Dioxide + *n*-Hexane), and (Carbon Dioxide + *n*-Heptane) at Temperatures *T* and CO_2 Mole Fraction x_1

	T/K				
x_1	293.15	298.15	303.15	308.15	313.15
	P_b/MPa (U_i %) CO_2 + Benzene				
0.510	3.43 (1.00)	3.83 (1.15)	4.24 (1.00)	4.56 (0.67)	4.88 (0.67)
0.602	3.89 (0.88)	4.29 (1.20)	4.78 (0.88)	5.21 (0.88)	5.58 (0.58)
0.710	4.31 (1.15)	4.84 (0.88)	5.24 (0.33)	5.73 (1.20)	6.28 (1.00)
0.803	4.61 (1.20)	5.14 (0.88)	5.59 (1.20)	6.21 (0.67)	6.82 (0.67)
0.908	4.98 (1.00)	5.62 (0.58)	6.15 (1.20)	6.81 (0.88)	7.42 (0.88)
	CO_2 + Methylbenzene				
0.502	3.68 (0.88)	3.80 (0.58)	4.21 (0.33)	4.50 (0.88)	4.92 (0.88)
0.601	4.06 (1.15)	4.53 (0.67)	4.88 (0.67)	5.40 (0.67)	5.82 (0.67)
0.707	4.42 (0.88)	5.03 (1.15)	5.46 (0.88)	6.01 (1.20)	6.51 (0.58)
0.808	4.81 (0.67)	5.30 (0.88)	5.95 (1.20)	6.39 (1.15)	7.05 (1.15)
0.903	4.93 (0.33)	5.58 (0.88)	6.29 (1.20)	6.91 (0.88)	7.49 (1.20)
	CO_2 + *n*-Hexane				
0.503	3.28 (0.58)	3.51 (0.67)	3.83 (0.88)	4.06 (0.67)	4.35 (0.88)
0.610	3.84 (0.88)	4.15 (1.20)	4.59 (1.20)	4.86 (1.00)	5.21 (0.58)
0.708	4.24 (0.58)	4.65 (0.88)	5.08 (0.67)	5.51 (0.58)	5.89 (1.20)
0.810	4.61 (1.15)	5.07 (0.33)	5.58 (0.88)	6.02 (1.20)	6.45 (0.67)
0.910	5.07 (0.67)	5.55 (0.88)	6.15 (0.67)	6.65 (1.20)	7.31 (0.88)
	CO_2 + *n*-Heptane				
0.503	3.48 (0.88)	3.79 (1.20)	4.11 (0.67)	4.32 (1.15)	4.57 (1.20)
0.605	4.12 (1.15)	4.42 (0.67)	4.76 (1.00)	5.18 (0.88)	5.43 (0.67)
0.707	4.53 (1.00)	4.92 (0.33)	5.41 (1.20)	5.82 (0.88)	6.29 (0.88)
0.802	4.81 (0.33)	5.28 (0.88)	5.78 (0.88)	6.31 (0.33)	6.91 (0.58)
0.904	5.09 (0.67)	5.61 (1.00)	6.14 (0.67)	6.78 (1.20)	7.41 (0.33)

Table 3. Correlated Bubble Point Pressure P_b for (Carbon Dioxide + Benzene), (Carbon Dioxide + Methylbenzene), (Carbon Dioxide + *n*-Hexane), and (Carbon Dioxide + *n*-Heptane) at Temperatures *T* and CO_2 Mole Fraction x_1

	T/K				
x_1	293.15	298.15	303.15	308.15	313.15
	P_b/MPa (ARD %) CO_2 + Benzene				
0.510	3.46 (0.87)	3.80 (0.78)	4.16 (1.89)	4.53 (0.66)	4.91 (0.61)
0.602	3.91 (0.51)	4.31 (0.47)	4.73 (1.05)	5.17 (0.77)	5.63 (0.90)
0.710	4.33 (0.46)	4.79 (1.03)	5.28 (0.76)	5.80 (1.22)	6.35 (1.11)
0.803	4.63 (0.43)	5.14 (0.00)	5.69 (1.79)	6.26 (0.81)	6.87 (0.73)
0.908	5.02 (0.80)	5.59 (0.53)	6.19 (0.65)	6.82 (0.15)	7.48 (0.81)
	CO_2 + Methylbenzene				
0.502	3.57 (2.99)	3.82 (0.53)	4.18 (0.71)	4.49 (0.22)	4.81 (2.24)
0.601	4.11 (1.23)	4.43 (2.21)	4.87 (0.20)	5.27 (2.41)	5.69 (2.23)
0.707	4.54 (2.71)	4.95 (1.59)	5.47 (0.18)	5.97 (0.67)	6.49 (0.31)
0.808	4.82 (0.21)	5.32 (0.38)	5.89 (1.01)	6.48 (1.41)	7.09 (0.57)
0.903	5.07 (2.84)	5.64 (1.08)	6.26 (0.48)	6.90 (0.14)	7.58 (1.20)
	CO_2 + *n*-Hexane				
0.503	3.27 (0.30)	3.53 (0.57)	3.81 (0.52)	4.08 (0.49)	4.36 (0.23)
0.610	3.83 (0.26)	4.16 (0.24)	4.51 (1.74)	4.86 (0.00)	5.22 (0.19)
0.708	4.25 (0.24)	4.65 (0.00)	5.06 (0.39)	5.49 (0.36)	5.92 (0.51)
0.810	4.62 (0.22)	5.09 (0.39)	5.57 (0.18)	6.06 (0.66)	6.57 (1.86)
0.910	5.02 (0.99)	5.56 (0.18)	6.12 (0.49)	6.69 (0.60)	7.27 (0.55)
	CO_2 + *n*-Heptane				
0.503	3.57 (2.59)	3.81 (0.53)	4.06 (1.22)	4.31 (0.23)	4.56 (0.22)
0.605	4.15 (0.73)	4.46 (0.90)	4.79 (0.63)	5.11 (1.35)	5.45 (0.37)
0.707	4.58 (1.10)	4.98 (1.22)	5.38 (0.55)	5.80 (0.34)	6.22 (1.11)
0.802	4.84 (0.62)	5.31 (0.57)	5.79 (0.17)	6.29 (0.32)	6.79 (1.74)
0.904	5.08 (0.20)	5.62 (0.18)	6.18 (0.65)	6.76 (0.29)	7.35 (0.81)

and the results are the average of the replicates. The estimated uncertainty[37] of each measurement for the binary systems used in this work was calculated and reported in Table 2.

Table 3 presents the results for the bubble point pressure of (carbon dioxide + benzene), (carbon dioxide + methylbenzene), (carbon dioxide + *n*-hexane), and (carbon dioxide + *n*-heptane) obtained from well-known cubic equations of state, the PR EOS with one binary interaction parameter, along with the ARD % of the PR EOS from the experimental data. A careful study of

Table 4. Peng−Robinson Equation of State Binary Interaction k_{ij} Parameters for (Carbon Dioxide + Benzene), (Carbon Dioxide + Methylbenzene), (Carbon Dioxide + *n*-Hexane), and (Carbon Dioxide + *n*-Heptane)

system	interaction parameter (k_{ij})	range of temperature (K)
CO_2 + benzene	$k_{12} = 0.1115 - 0.1021 \cdot 10^{-3}T$	
CO_2 + methylbenzene	$k_{12} = 0.2676 - 0.6007 \cdot 10^{-3}T$	$293.15 \le T \le 313.15$
CO_2 + *n*-hexane	$k_{12} = 0.1692 - 0.2002 \cdot 10^{-3}T$	
CO_2 + *n*-heptane	$k_{12} = 0.3282 - 0.7015 \cdot 10^{-3}T$	

Tables 2 and 3 reveals that the result obtained from the PR EOS can accurately correlate the bubble point pressure data at different temperatures. The percent of AARDs of bubble point pressure for the binary systems of (carbon dioxide + benzene), (carbon dioxide + methylbenzene), (carbon dioxide + *n*-hexane), and (carbon dioxide + *n*-heptane) was found to be 0.79 %, 1.19 %, 0.49 %, and 0.75 %, respectively.

It should be stated that only one binary interaction parameter was considered to be an adjustable parameter in correlating the experimental data using the PR EOS and that the values for the binary interaction parameters at different temperatures for each system were regressed and reported in Table 4.

In the case of (carbon dioxide + benzene) and (carbon dioxide + *n*-hexane), the experimental results obtained from the PVT apparatus at (298.15 and 313.15) K were compared with those reported by Ohgaki and Katayama[13] in Figures 2 and 4. The comparison showed that the percent of AARDs of bubble point pressure for the binary systems of (carbon dioxide + benzene) and (carbon dioxide + *n*-hexane) at (298.15 and 313.15) K are (4.61 % and 5.15 %) and (5.49 % and 5.03 %), respectively.

In the case of (carbon dioxide + benzene), the experimental results obtained from the PVT apparatus at $T = 313.15$ K were compared with those reported by Gupta et al.[14] in Figure 2. The comparison showed that for such systems the percent of AARD of bubble point pressure at 313.15 K is 2.32 %. Also, the experimental results for (carbon dioxide + *n*-hexane) obtained from the PVT apparatus at $T = 313.15$ K were compared with those reported by Li et al.[28] in Figure 4. The comparison showed that for such systems the percent of AARD of bubble point pressure at 313.15 K is 0.95 %.

The correlated bubble point pressure for (carbon dioxide + benzene) and (carbon dioxide + *n*-hexane) was compared with

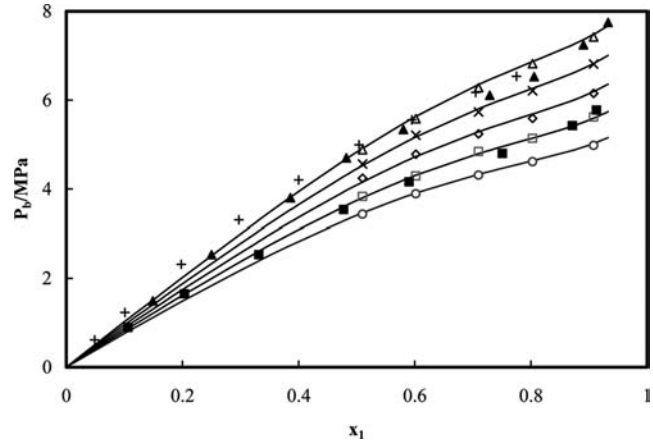

Figure 2. Experimental and correlated bubble pressure P_b for (carbon dioxide + benzene) as a function of CO_2 mole fraction x_1 at temperatures ranging from (293.15 to 313.15) K. ○, this work at $T = 293.15$ K; □, this work at $T = 298.15$ K; ■, ref 13 at $T = 298.15$; ◇, this work at $T = 303.15$ K; ×, this work at $T = 308.15$ K; Δ, this work at $T = 313.15$ K; ▲, ref 13 at $T = 313.15$; +, ref 14 at $T = 313.15$ K; −, PR EOS at temperatures ranging from (293.15 to 313.15) K.

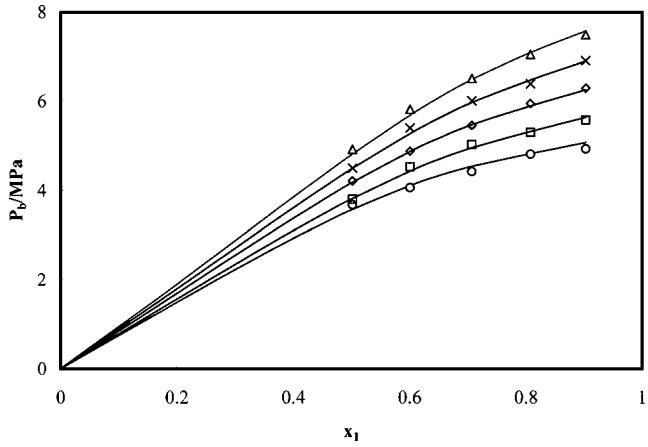

Figure 3. Experimental and correlated bubble pressure P_b for (carbon dioxide + methylbenzene) as a function of CO_2 mole fraction x_1 at temperatures ranging from (293.15 to 313.15) K. ○, this work at $T = 293.15$ K; □, this work at $T = 298.15$ K; ◇, this work at $T = 303.15$ K; ×, this work at $T = 308.15$ K; Δ, this work at $T = 313.15$ K; −, PR EOS at temperatures ranging from (293.15 to 313.15) K.

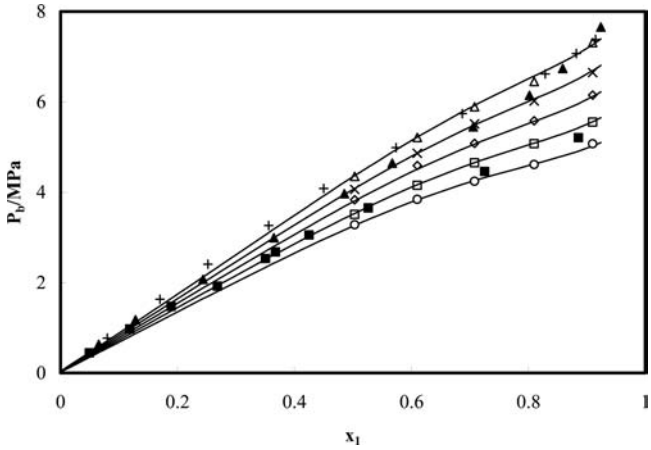

Figure 4. Experimental and correlated bubble pressure P_b for (carbon dioxide + *n*-hexane) as a function of CO_2 mole fraction x_1 at temperatures ranging from (293.15 to 313.15) K. ○, this work at $T = 293.15$ K; □, this work at $T = 298.15$ K; ■, ref 13 at $T = 298.15$; ◇, this work at $T = 303.15$ K; ×, this work at $T = 308.15$ K; Δ, this work at $T = 313.15$ K; ▲, ref 13 at $T = 313.15$; +, ref 28 at $T = 313.15$; −, PR EOS at temperatures ranging from (293.15 to 313.15) K.

those reported by Ohgaki and Katayama[13] at temperatures of (298.15 and 313.15) K. The percent of AARDs of bubble point pressure for (carbon dioxide + benzene) and (carbon dioxide + *n*-hexane) at temperatures of (298.15 and 313.15) K are (2.04 % and 2.14 %) and (4.98 % and 5.32 %), respectively.

In the case of (carbon dioxide + *n*-heptane), the correlated bubble point pressure for such a system was compared with those reported by Mutelet et al.[34] at 310.65 K in Figure 5. The comparison showed that the percent of AARD of bubble point pressure at 310.65 K is 2.04 %.

Conclusion

The bubble point pressures of (carbon dioxide + benzene), (carbon dioxide + methylbenzene), (carbon dioxide + *n*-hexane), and (carbon dioxide + *n*-heptane) were measured at carbon dioxide mole fractions from 0.502 to 0.91, and within the temperature range of (293.15 to 313.15) K. The bubble point pressure for each binary system increases with increasing mole fraction of CO_2 at constant temperature. As seen from Figures 2 through 5, the PR EOS with only one interaction parameter

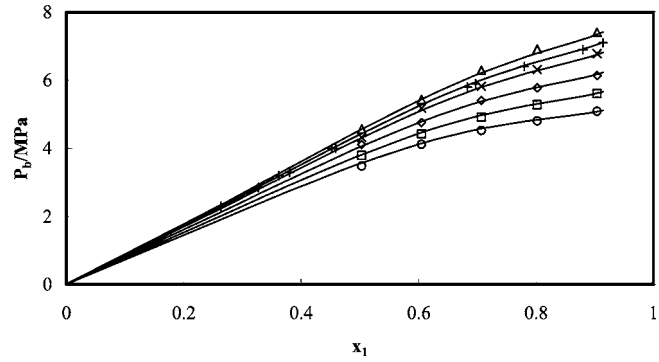

Figure 5. Experimental and correlated bubble pressure P_b for (carbon dioxide + *n*-heptane) as a function of CO_2 mole fraction x_1 at temperatures ranging from (293.15 to 313.15) K. ○, this work at $T = 293.15$ K; □, this work at $T = 298.15$ K; ◇, this work at $T = 303.15$ K; ×, this work at $T = 308.15$ K; +, ref 34 at $T = 310.65$; Δ, this work at $T = 313.15$ K; −, PR EOS at temperatures ranging from (293.15 to 313.15) K.

was used in correlating the experimental data generated in this work. The results showed that the PR EOS can accurately correlate the experimental data for the bubble point pressure at different temperatures.

The results showed that carbon dioxide can be dissolved readily in benzene, methylbenzene, *n*-hexane, and *n*-heptane at elevated pressures. At temperature of (293.15 to 298.15) K and pressure higher than 4 MPa, the liquid phase is mostly carbon dioxide, and such behavior can be observed at higher pressure with increasing temperature. These conditions are considered to be appropriate in the supercritical fluid processes to produce microparticles as well as nanoparticles.

Literature Cited

(1) Matson, D. W.; Fulton, J. L.; Petersen, R. C.; Smith, R. D. Rapid Expansion of Supercritical Fluid Solutions: Solute Formation of Powders, Thin Film and Fibers. *Ind. Eng. Chem. Res.* **1987**, *26*, 2298–2306.

(2) Chattopadhyay, P.; Gupta, R. B. Production of Antibiotic Nanoparticles Using Supercritical CO_2 as Antisolvent with Enhanced Mass Transfer. *Ind. Eng. Chem. Res.* **2001**, *40*, 3530–3539.

(3) Kikic, I.; Lora, M.; Bertucco, A. Thermodynamic Analysis of Three-Phase Equilibria in Binary and Ternary Systems for Applications in Rapid Expansion of a Supercritical Solution (RESS), Particles from Gas-Saturated Solutions (PGSS) and Supercritical Antisolvent Crystallization (SAS). *Ind. Eng. Chem. Res.* **1997**, *36*, 5507–5515.

(4) Cocero, M. J.; Ferrero, S. Crystallization of β-carotene by a GAS Process in Batch: Effect of Operating Parameters. *J. Supercrit. Fluids* **2002**, *22*, 237–245.

(5) Kalogiannis, C. G.; Eleni, P.; Panayiotou, C. G. Production of Amoxicillin Microparticles by Supercritical Antisolvent Precipitation. *Ind. Eng. Chem. Res.* **2005**, *44*, 9339–9346.

(6) Bleich, J.; Muller, B. W. Production of Drug Loaded Microspheres by the Use of Supercritical Gases with the Aerosol Solvent Extraction System (ASES) Process. *J. Microencapsul.* **1996**, *13*, 131–139.

(7) York, P. Strategies for Particle Design Using Supercritical Fluid Technologies. *Pharm. Sci. Technol. Today* **1999**, *2*, 430–440.

(8) de la Fuente, J. C.; Peters, C. J.; de Swaan Aronsqq, J. Volume Expansion in Relation to the Gas Antisolvent Process. *J. Supercrit. Fluids* **2000**, *17*, 13–23.

(9) Chang, J. C.; Randolph, A. D. Solvent Expansion and Solute Solubility Predictions in Gas-Expanded Liquids. *AIChE J.* **1990**, *36*, *6*, 939–942.

(10) Mukhopadhyay, M.; Dalvi, S. V. Partial Molar Volume Fraction of Solvent in Binary (CO_2-Solvent) Solution for Solid Solubility Predictions. *J. Supercrit. Fluids* **2004**, *29*, *3*, 221–230.

(11) Kim, C. H.; Vimalchand, P.; Donohue, M. D. Vapor-Liquid Equilibria for Binary Mixtures of Carbon Dioxide with Benzene, Methylbenzene and p-Xylene. *Fluid Phase Equilib.* **1986**, *31*, 299–311.

(12) Nemati Lay, E.; Taghikhani, V.; Ghotbi, C. Measurement and Correlation of CO2 Solubility in the Systems of CO2/Methylbenzene, CO2/Benzene, and CO2/n-Hexane at Near-Critical and Supercritical Conditions. *J. Chem. Eng. Data* **2006**, *51*, 2197–2200.

(13) Ohgaki, K.; Katayama, T. Isothermal Vapor-Liquid Equilibrium Data for Binary Systems Containing Carbon Dioxide at High Pressures: Carbon Dioxide/Methanol, Carbon Dioxide/n-Hexane, and Carbon Dioxide/Benzene Systems. *J. Chem. Eng. Data* **1976**, *21*, 53–55.
(14) Gupta, M. K.; Li, Y. H.; Huisey, B. J.; Robinson, R. L., Jr. Phase Equilibrium for Carbon Dioxide/Benzene at 313.2, 353.2, and 393.2 K. *J. Chem. Eng. Data* **1982**, *27*, 55–57.
(15) Nagarajan, N.; Robinson, R. L., Jr. Equilibrium Phase Composition, Phase Densities, and Interfacial Tensions for CO_2/Hydrocarbon Systems, CO_2/Cyclohexane and CO_2/Benzene. *J. Chem. Eng. Data* **1987**, *32*, 369–371.
(16) Inomata, H.; Arai, K.; Saito, S. Vapor-Liquid Equilibria for Carbon Dioxide/Hydrocarbon Mixtures at Elevated Temperatures and Pressures. *Fluid Phase Equilib.* **1987**, *36*, 107–119.
(17) Kaminishi, G. I.; Yokoyama, C.; Takahashi, S. Vapor Pressures of Binary Mixtures of Carbon Dioxide with Benzene, n-Hexane and Cyclohexane up to 7 MPa. *Fluid Phase Equilib.* **1987**, *34*, 83–99.
(18) Zhiyi, L.; Weili, W.; Xiaodong, Z.; Xuewu, L.; Dapeng, H.; Yuanjing, X. Vapor-Liquid Phase Behavior of the Binary Systems Containing Supercritical Carbon Dioxide. *Chem. Eng. Process.* **2004**, *43*, 541–545.
(19) Ng, H. J.; Robinson, D. B. Equilibrium Phase Properties of the Methylbenzene/Carbon Dioxide System. *J. Chem. Eng. Data* **1978**, *23*, 325–327.
(20) Sebastian, H. M.; Simnick, J. J.; Lin, H. M.; Chao, K. C. Gas-Liquid Equilibrium in Mixture of Carbon Dioxide/Methylbenzene and Carbon Dioxide/m-Xylene. *J. Chem. Eng. Data* **1980**, *25*, 246–248.
(21) Tochigi, K.; Hasegawa, K.; Asano, N.; Kojima, K. Vapor-Liquid Equilibria for the Carbon Dioxide/Pentane and Carbon Dioxide/Methylbenzene Systems. *J. Chem. Eng. Data* **1998**, *43*, 954–956.
(22) Morris, W. O.; Donohue, M. D. Vapor-Liquid Equilibria in Mixtures Containing Carbon Dioxide, Methylbenzene, and 1-Methylnaphthalene. *J. Chem. Eng. Data* **1985**, *30*, 259–263.
(23) Wu, W.; Ke, J.; Poliakoff, M. Phase Boundaries of CO_2/Methylbenzene, CO_2/Acetone, and CO_2/Ethanol at High Temperatures and High Pressures. *J. Chem. Eng. Data* **2006**, *51*, 1398–1403.
(24) Chang, C. J. The Solubility of Carbon Dioxide in Organic Solvents at Elevated Pressures. *Fluid Phase Equilib.* **1992**, *74*, 235–242.
(25) Chang, C. J. Volume Expansion Coefficients and Activity Coefficients of High-Pressure Carbon Dioxide Dissolution in Organic Liquids at 298 K. *J. Chem. Eng. Jpn.* **1992**, *25*, 164–170.
(26) Naidoo, P.; Ramjugernath, D.; Raal, J. D. A New High-Pressure Vapor-Liquid Equilibrium Apparatus. *Fluid Phase Equilib.* **2008**, *269*, 104–112.
(27) Wagner, Z.; Wichterle, I. High-Pressure Vapor-Liquid Equilibrium in Systems Containing Carbon Dioxide, 1-Hexene, and n-Hexane. *Fluid Phase Equilib.* **1987**, *33*, 109–123.
(28) Li, Y. H.; Dillard, K. H.; Robinson, R. L., Jr. Vapor-Liquid Phase Equilibrium for Carbon Dioxide/n-Hexane at 40, 80 and 120 deg C. *J. Chem. Eng. Data* **1981**, *26*, 53–55.
(29) Chen, D.; Chen, W. Phase Equilibria of n-Hexane and n-Octane in Critical Carbon Dioxide. *Huaxue Gongcheng* **1992**, *20*, 66–69.
(30) Choi, E. J.; Yeo, S. D. Critical Properties for Carbon Dioxide/n-alkane Mixtures Using a Variable-Volume View Cell. *J. Chem. Eng. Data* **1998**, *43*, 714–716.
(31) Kalra, H.; Kubota, H.; Robinson, D. B.; Ng, H. J. Equilibrium Phase Properties of the Carbon Dioxide/n-Heptane system. *J. Chem. Eng. Data* **1978**, *23*, 317–321.
(32) Hayduk, W.; Walter, E. B.; Simpson, P. Solubility of Propane and Carbon Dioxide in Heptane, Dodecane, and Hexadecane. *J. Chem. Eng. Data* **1972**, *17*, 59–61.
(33) Fenghour, A.; Trusler, J. P. M.; Wakeham, W. A. Densities and Bubble Points of Binary Mixtures of Carbon Dioxide and n-Heptane and Ternary Mixtures of n-Butane, n-Heptane, and n-Hexadecane. *Fluid Phase Equilib.* **2001**, *185*, 349–358.
(34) Mutelet, F.; Vitu, S.; Privat, R.; Jaubert, J.-N. Solubility of CO_2 in Branched Alkanes in Order to Extend the PPR78 Model (Predictive 1978, Peng Robinson EOS with Temperature-Dependent k_{ij} Calculated Through a Group Contribution Method) to Such Systems. *Fluid Phase Equilib.* **2005**, *238*, 157–168.
(35) Kho, Y. W.; Conrad, D. C.; Knutson, B. L. Phase Equilibria and Thermophysical Properties of Carbon Dioxide/Expanded Fluorinated Solvents. *Fluid Phase Equilib.* **2003**, *206*, 179–193.
(36) Peng, D.; Robinson, D. B. A New Two-Constant Equation of State. *Ind. Eng. Chem. Fundam.* **1976**, *5*, 59–64.
(37) Taylor, B. N.; Kuyatt, C. E. *Guidelines for the Evaluation and Expression of Uncertainty in NIST Measurement Results*; NIST Technical Note 129; National Institute of Standards and Technology: Gaithersburg, MD, 1994.

Received for review March 29, 2009. Accepted July 16, 2009.

JE900312Z